

JELENA M. JAKŠIĆ<sup>1,2</sup>  
LJILJANA M. VRAČAR<sup>1</sup>  
STYLIANOS G.  
NEOPHYTIDES<sup>2</sup>  
NEDELJKO V. KRSTAJIĆ<sup>1</sup>

<sup>1</sup>Faculty of Technology  
and Metallurgy, University  
of Belgrade, Belgrade,  
Serbia and Montenegro

<sup>2</sup>Institute of Chemical  
Engineering and High  
Temperature Chemical  
Processes, FORTH,  
Patras, Greece

SCIENTIFIC PAPER

669.28'231:536.717:531.3

## STRUCTURAL EFFECTS ON KINETIC PROPERTIES FOR HYDROGEN ELECTRODE REACTIONS AND CO TOLERANCE ALONG Mo-Pt PHASE DIAGRAM

The effect of structural and surface versus bulk properties of Mo-Pt alloys and intermetallic phases taken along their phase diagram upon kinetic and electrocatalytic features for the cathodic hydrogen evolution (HER) has been thoroughly investigated and displayed. All specimens along Mo-Pt phase diagram in broader reversible potential range feature Volmer-Tafel mechanism with the catalytic recombination of Tafel as the rate-determining step (RDS), while further polarization plot in semi logarithmic (vs. log) system shows Volmer-Heyrowski mechanism with the electrochemical desorption of Heyrowski reaction being the RDS; the extension of the former depends on the degree of MoO<sub>3</sub> coverage and blocking active centers of electrode surface. XPS, UPS, XRD and work function characterization of all specimens revealed congenial volcano plots relative to the same dependence in electrocatalysis. As the main observation the most stable and prevailing Pt content specimens feature the best electrocatalytic and kinetic properties. Activated (MoO<sub>3</sub> free) MoPt<sub>3</sub> and MoPt<sub>4</sub> catalysts feature all along the Tafel plot reversible Tafel catalytic reaction as the RDS, and create properties of super-activity within a broader current density range. It has been pointed out that an intermetallic phase with prevailing Mo atomic percentage (MoPt<sub>3</sub>) features pronounced electrocatalytic properties for the HER.

Key words: electrocatalysis, hydrogen evolution reaction, Mo-Pt alloys, intermetallic phases.

Platinum so far has been the best electrocatalyst for both anodic hydrogen oxidation and cathodic oxygen reduction in Low Temperature PEM Fuel Cells (LT PEM FC). However, its low CO tolerance (up to 20 ppm) [1] and intention for at least partial replacement of noble by other cheaper and wider disseminated transition metals, and in particular a broader search for synergistic electrocatalytic effects, imposed long ago catalytic trends towards composite alloyed electrocatalysts. In such a respect, it has been shown theoretically and proved by plentiful of experimental evidence that hypo-hyper-*d*-interelectronic combinations of transition metals, mostly symmetric and stable Laves intermetallic phases, almost without exception, feature synergism in their electrocatalytic behavior for the cathodic hydrogen evolution (HER) [2,3].

Ever since Watanabe [4] has pointed out that an alloying combination of Ru and Pt succeeds to shift the peak of primary oxide (M-OH) growth towards more negative potential values along the anodic scan of voltammogram, the search for oxophilic components (Fig. 1) [5] has been the main trend in development of CO tolerant electrocatalysts for LT PEM FC. The ones of most successful and cheaper combinations so far have been MoPt<sub>3</sub> and MoPt<sub>4</sub> [6-9].

The aim of the present paper would be to investigate and characterize surface versus bulk structure of alloys and intermetallic phases along Mo-Pt phase diagram and then to undertake kinetic measurements for the HER with such a defined model system as a standard etalon for all further comparisons

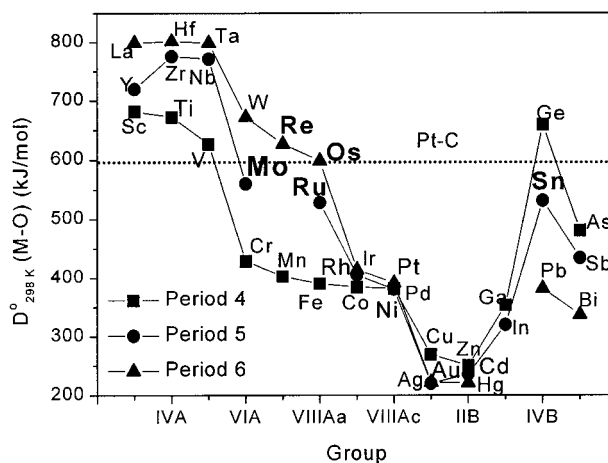


Figure 1. The metal-oxygen bond dissociation energy [ $D_{298K}^0(M-O)$ ] in diatomic molecules as a function of group in the Periodic Table [5]. The horizontal dotted line represents the Pt-C bond. The idea was to match the same M-O to the Pt-C bond in the Smotkin concept (courtesy by E. Smotkin).

in electrocatalysis. The search for correlations between surface and electronic state versus its bulk composition and electrocatalytic properties would be a particular leading task, too.

### EXPERIMENTAL

Specimens of *a priori* defined interatomic composition along Mo-Pt phase diagram were produced by arc-melting of high purity individual components (Mo 99.95, Pt 99.99 wt.%) under argon protecting atmosphere (Philips Research Laboratory, Eindhoven, Holland), followed by longer annealing at 1100°C.

Author address: J.M. Jakšić, Faculty of Technology and Metallurgy, University of Belgrade, Karnegijeva 4, Belgrade, Serbia and Montenegro

E-mail: milan@iceht.forth.gr

Paper received and accepted: April 7, 2005

Phase composition, atomic ratio of interbonding components and structural parameters of crystal lattice were analyzed by XRD scans (Philips PW-1050 diffractometer, which uses Cu-K $\alpha$  rays), before and after electrochemical measurements.

Electronic state of all samples was studied by XPS analysis. XP spectra were collected in an UHV chamber (base pressure  $8 \times 10^{-10}$  mbar), equipped with a hemispherical electron energy analyzer and a twin anode X-ray gun and a UV-lamp described elsewhere in more details [10]. The sample, which was mounted on a transfer rod probe, could be easily transferred from the load lock chamber, where it could be treated with gases at atmospheric pressure and elevated temperatures, into the UHV chamber. The unmonochromatized Al K $\alpha$  line at 1486.6 eV and the He II line at 40.8 eV with a constant pass energy mode for the analyzer were used in the XPS and UPS experiments, respectively. Pass energies of 97 eV resulted in a half width at the half maximum (FWHM) of 1.8 eV for the Au 4f $_{7/2}$  peak of a reference foil. The energy scale of the spectrometer was calibrated with both the Au 4f $_{7/2}$  line at 84.0 eV, and the Ni 2p $_{3/2}$  line at 852.4 eV of carefully cleaned polycrystalline Au and Ni foils, respectively. The sample temperature was measured with a Ni-CrNi thermocouple, which was mounted in the sample holder. Curve fitting was performed with least-squares curve-fitting program based on a mixed Gaussian/Lorentzian function, which accounted for the band asymmetry to higher binding energies in the core level spectra of metallic species. All spectra were obtained at room temperature, after heating the sample at 570 K under H $_2$  atmosphere for 30 min and the binding energies (BE) are referenced to C1s line at 284.6 eV, which was always present due to unavoidable carbon contamination. The uncertainty in the determination of the binding energy values was estimated to be 0.1 eV while being in calculated atomic ratios of about 10%. The objective of the XPS measurements was to detect possible intermetallic bonding of hypo-hyper-*d*-interelectronic combinations of Mo and Pt and their oxides. UPS measurements along with Kelvin probe were used to assess work function of specimens along with the Fermi energy.

All samples were thoroughly prepared and brought to the same roughness factor (about 1.8), as a constant denominator in current density and thereby the same available surface area enabling to be straightforward comparable in polarization measurements. The roughness factor has been assessed by the double layer capacitance measurements with the assumption that for absolutely smooth surface it amounts 20  $\mu\text{F}\cdot\text{cm}^{-2}$ , and from hydrogen desorption peaks in cyclic voltammetry (CV) compared with pure Pt at its full coverage (250  $\mu\text{C}\cdot\text{cm}^{-2}$ ). All kinetic measurements were carried out at 298 K in a typical three-compartment electrochemical glass cell, electrolytically connected by porous frit, with

both stationary and rotating disk working electrode (RDE, 0 – 2500 rpm), kept under pure hydrogen gas along with RHE as the reference electrode. All specimen electrodes were thoroughly cleaned and longer prepolarized at 100  $\text{mA}\cdot\text{cm}^{-2}$  before each polarization scan. Measurements were carried out in 0.5 M HClO $_4$  solution prepared from BDH 'Aristar'– and water of nano-degree-purity, the latter being always checked and confirmed by Pt cyclic voltammogram, as compared with its calibration etalon from reliable literature [11,12]. Temperature dependence of H-adsorption from CV and ac impedance to complete the kinetic picture and were also measured and published elsewhere [13–15].

Steady-state polarization measurements were performed with a constant increment in cathodic potential changes and with equal time duration (60 sec) at each point, this way enabling to be established corresponding steady values of current density, starting at – 0.150 V vs. RHE after longer prepolarization, and ending at the open circuit potential, that means to cover the range from 1.0  $\mu\text{A}\cdot\text{cm}^{-2}$  till 100  $\text{mA}\cdot\text{cm}^{-2}$  while recording Tafel plots,  $\eta = f(\log j)$ . In such a respect two types of measurements were carried out: (a) With *activated electrode* freshly repolished at the finest degree of treatment with 0.05  $\mu\text{m}$  alumina powder, and (b) Clean electrode after longer (60 min) cathodic prepolarization at –0.150 V vs. RHE, ohmic drop being properly subtracted.

Nanostructured Pt/TiO $_2$  and MoPt $_x$ /TiO $_2$  were prepared *via* wet impregnation of Pt and MoO $_2$  acetylacetonates (2,4-pentanedionates) on TiO $_2$  anatase (Hombikat Schtleben, surface area 200  $\text{m}^2/\text{g}$ ) [16,17]. After drying, the catalyst precursors were loaded in the DRIFTS reactor cell and treated in flowing H $_2$ /Ar stream by varying temperature with a ramp rate of 2 K/min up to 573 K, where the sample was kept for 2 hours. After such a thermal treatment, the sample was cooled down to room temperature under the same gas and ramp rate. The Pt/TiO $_2$  and MoPt $_x$ /TiO $_2$  were prepared with a constant metal loading of 5 wt.%. Two specimens with Mo/Pt atomic ratios  $x = 1.4$  were investigated, while monometallic 5 wt.% Pt/TiO $_2$  and Mo/TiO $_2$  were prepared the same way and measured for comparison [16,17].

## RESULTS AND DISCUSSION

### XPS Surface versus Bulk Characterization

The main surface electrode characterization concerns surface relative to the bulk composition, since electrocatalytic processes bear the same properties of heterogeneous catalysis, and consequently primarily depend on the state of surface structure where electrochemical reactions take place.

Brewer [18,19] and Miedema [20] intermetallic bonding models and Friedel [21,22] *d*-*d*-correlations a

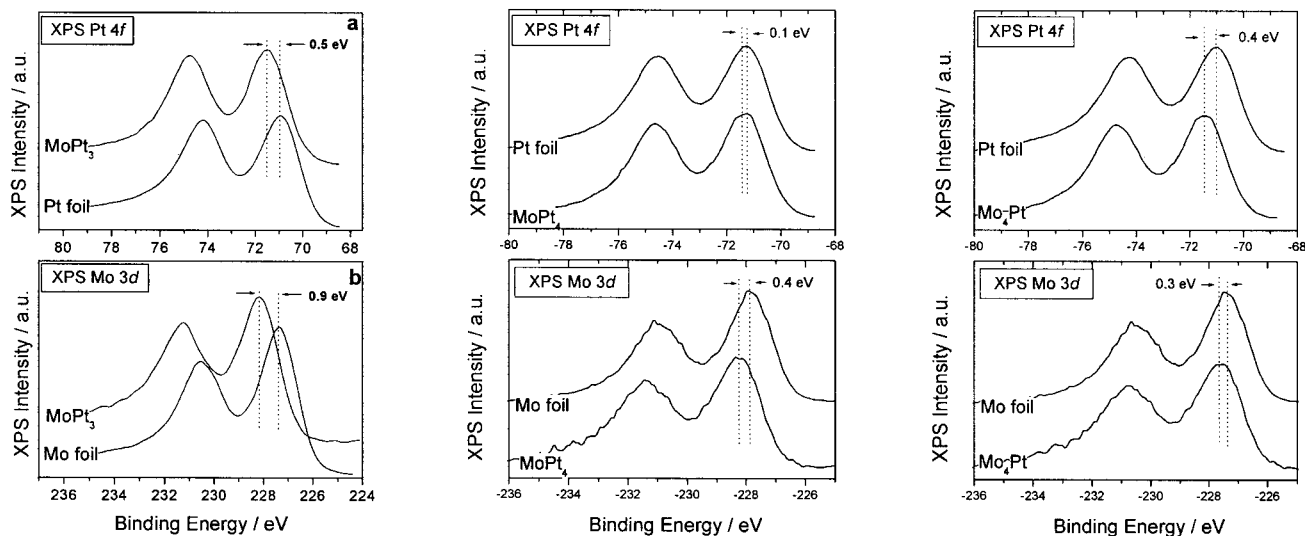


Figure 2. Comparative XP spectrum of the Pt 4f (a) and Mo 3d region (b) of  $\text{MoPt}_3$ ,  $\text{MoPt}_4$  and  $\text{Mo}_4\text{Pt}$ , along with pure individual Mo and Pt foil samples.

*priori* predict for such a hypo-hyper-*d*-interelectronic Mo-Pt system rather strong bonding and the existence of extra-stable intermetallic phases, while the existing theoretical inference consequently implies pronounced high synergistic electrocatalytic effects for the HELR [2,3]. In such a context, primarily in accordance with the Brewer intermetallic bonding theory [18,19], XPS analysis reveals (Fig. 2), the remarkable shift of the bonding peak of both Pt and Mo all along the phase diagram (Fig. 3). This in particular concerns the most symmetric and most stable Laves phase  $\text{MoPt}_3$ , when compared with the meta stable  $\text{MoPt}_4$  (Fig. 2, a & b). There is a strong indication of *d*-electron transfer from hyper-*d*-electronic Pt (antibonding band) to the deficient hypo-*d*-electronic Mo bonding band, though at rather high Mo contents, there are signs of the

opposite in the *d-d*-interelectronic transfer (Fig. 2 and 3). In fact, while the Brewer intermetallic bonding theory [18,19] is based on the transfer of paired *d*-electrons from hyper-*d*-orbitals upon partially empty hypo-*d*-band, Miedema model [20] implies the opposite direction in electron transfer for hypo-hyper-*d-d*-interelectronic bonding interaction. Such XPS analysis affords reliable indications, besides Brewer high temperature thermodynamics [18,19], that hypo-hyper-*d*-intermetallic bonding is primarily based on the partial *d*-electron delocalization within the interionic transfer.

After thorough  $\text{He}^-$  - ionic sputtering in the UHV chamber with the aim to remove surface blocking Mo-oxides, all specimens reveal the same surface composition that corresponds to their bulk structure (Fig. 4).

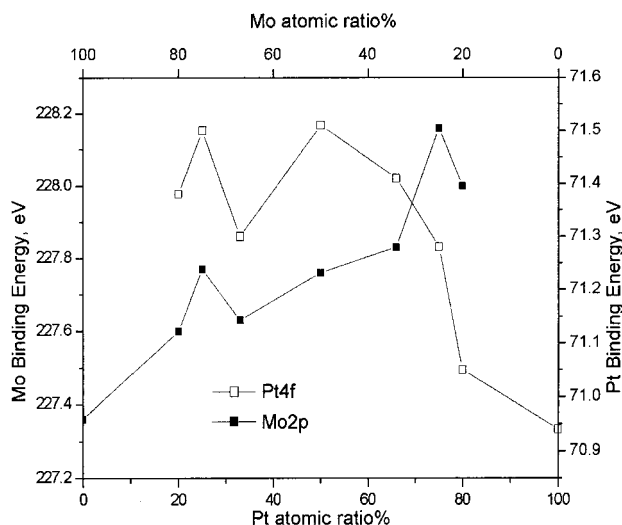


Figure 3. Variations of the Mo  $3d_{3/2}$  and Pt  $4f_{7/2}$  binding energies as a function of Pt-Mo atomic ratio.

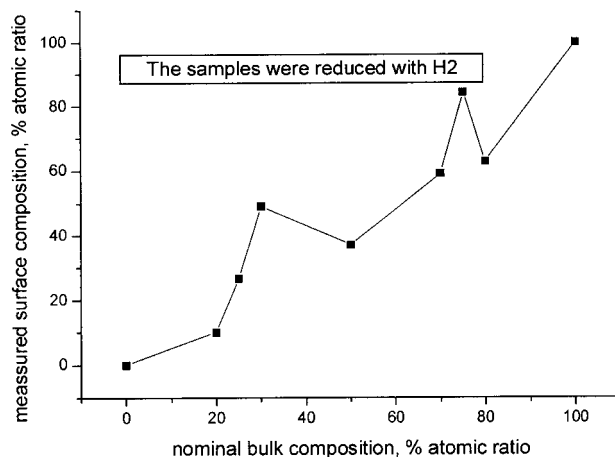


Figure 4. Dependence of surface versus bulk atomic mass ratio of prepared selected specimens, as obtained from nominal composition confirmed by XRD analysis and XPS measurements along Mo-Pt phase diagram.

Recent approach in the density functional theory [23–25], uses the  $d$ -band center ( $\epsilon_d$ ), as a parameter which measures the energy of the metal  $d$ -states relative to the Fermi energy, to establish the energy of segregation of alloying transition metals and therefrom the adsorption of H-adatoms [23] or CO [24,25]. The conclusions are quite the same as in the present theoretical considerations, since segregation is a reciprocal function of cohesive  $d$ - $d$ -bonding effectiveness and/or the  $d$ -band energy: chemisorption of H-adatoms decreases with decreasing segregation energy and in the same relation increases the electrocatalytic activity for the HER [23]. Such theory predicts that prevailing hyper- $d$ -metal, as a host, strongly pulls inside the phase hypo- $d$ -constituent of such an alloying composition and the attracting force depends on their intermetallic bonding affinity [24,25]. Interactions within two transition metals  $d$ -bands arises metal-dependent and treated as perturbation [23]. Qualitatively there is no difference with the present theoretical statements. However, the one thing is the hypo-hyper- $d$ -intermetallic bonding or its energy of segregation, and the resulting adsorption of H-adatoms, and quite another when the former comes in contact with oxygen and water molecules. The latter implies another type of strong interaction with otherwise oxophilic hypo- $d$ -ingredients and imposes an attraction to pull them back in opposite direction, to segregate as oxides upon the surface. The highest oxide valence states, in particular MoO<sub>3</sub>, block active catalytic centers and decrease the overall catalytic activity, while lower oxide states {MoO<sub>2</sub>, MoO(OH)<sub>3</sub> or MoO<sub>2</sub>(OH)} (usually exhibit electronic conductivity, rather high catalytic activity and spillover of the primary oxides (M–OH).

In the same respect, there has also been of deeper fundamental interest and significance to scan the work function changes along the Mo–Pt phase diagram (Fig. 5),

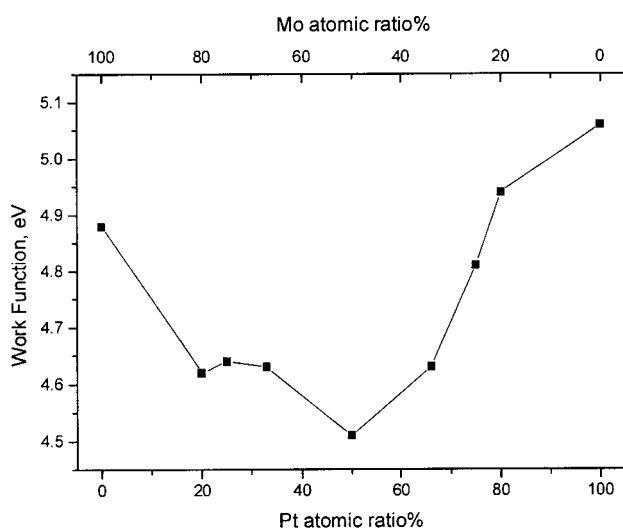


Figure 5. Shift of work function with Mo–Pt atomic ratio for various alloys and intermetallic phases.

as based upon UPS and Kelvin probe measurements, the two values coinciding within the range of experimental error. As theoretically predicted [26,27], the latter follows a characteristic reverse volcano plot, in which all values for alloys and intermetallic phases are lower than work function of initial individual constituents. Qualitatively such state of experimental evidence basically would correspond to the expectancies in electrocatalysis: the lower the work function, the more ease electron release, and consequently the higher the electrocatalytic activity. However, experimental evidence for individual transition elements follows an opposite volcanic correlation: maximum in work function volcano plots (Ni, Pd, Pt) coincides with the same maximum and follows the same shape of curve in electrocatalytic activity for the HER [26,27].

It is also evident that the higher the CO tolerance, the lower the work function [6–8]. In such a context, for example, Fe has a low work function and almost no CO adsorption at room temperature, in contrast to Pt, that features both a high work function and rather strong CO adsorptive bonding [1]. Such state of evidence suggests the correlation between work function and CO adsorption. This is associated with the oxophilicity changes in various hypo-hyper- $d$ -electronic combinations, and such a substantial decrease in work function enables the higher CO tolerance (Fig. 1).

### Characteristics of Mo–Pt Phase Diagram

Mo as a hypo- $d$ -electronic transition element with five semi-filled semi- $d$ -orbitals, which affords maximal number of reacting electrons, in combination with hyper- $d$ -electronic Pt, at the upper- $d$ -level and with 4 $d$ -electrons within the anti-bonding band, *a priori* suggests rather strong intermetallic bonding effectiveness. Such state manifests in a rather refractory high solidus–liquidus line, which extends between 2045 K for Pt and 2890 K for pure Mo (Fig. 6) [28]. There are five

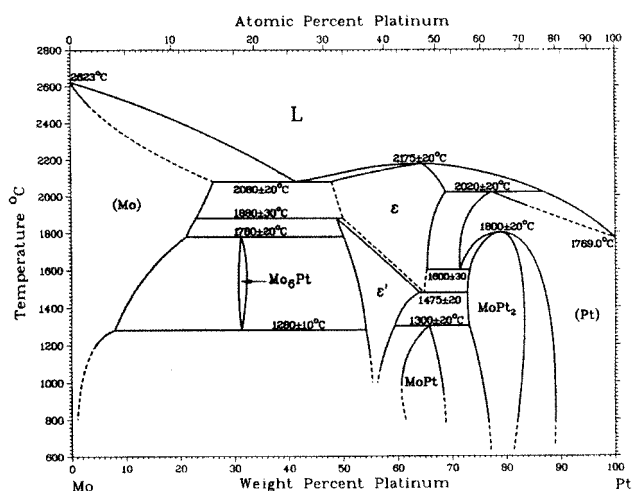


Figure 6. Equilibrium phase diagram of Mo–Pt system [28].

well defined intermetallic phases along Mo–Pt phase diagrams and thermodynamic data exist for each of them, but with uncertainties for enthalpy values, since activity coefficients sharply increase at lower temperature range.

### XRD Characterization of Mo–Pt Alloys and Intermetallic Phases

Between body (*bcc*) and face (*fcc*) centered cubic structure of Mo versus Pt, respectively, with prevailing noble metal content while alloying, for MoPt<sub>3</sub> and MoPt<sub>4</sub>, as predicted by the Brewer intermetallic bonding model [18,19], there follows a typical regular Laves monophasic polycrystalline *fcc* symmetry (Fig. 7). Along with Pt reference state (PDF 04–0802; *cF4*; Cu–type  $a_{\text{ref}} = 3.92 \text{ \AA}$ ) introduced for comparison, all major peaks of these three specimens are explained by such a *fcc* structure with somewhat smaller lattice constant than for the reference Pt state ( $a = 3.90 \text{ \AA}$ ). Such experimental evidence is not surprising since the elemental radii of W, Mo, and Pt are rather close each to other (approx.  $1.4 \text{ \AA}$ ), while these intermetallic phases grow with a rather high affinity and result as extra-stable with rather high enthalpies. Since the most stable MoPt<sub>3</sub> reveals an extra reflection at 29.5 degrees  $2\theta$  ( $d$ -value =  $3.02 \text{ \AA}$ ), the actual crystal structure in these two specimens is likely to be either a superstructure of the *fcc* phase, or a less symmetric structure of the *fcc* lattice.

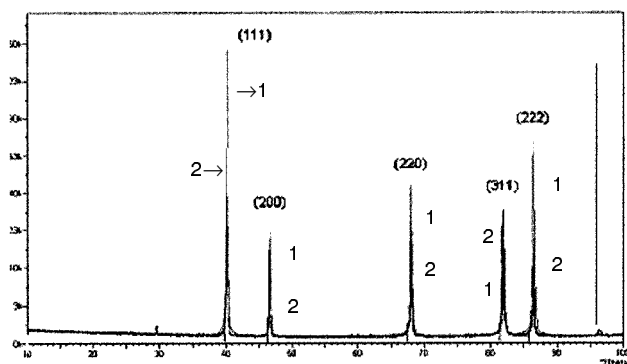


Figure 7. XRD diffractograms of MoPt<sub>3</sub> (1), and MoPt<sub>4</sub> (2) along with the reference state of pure Pt.

The middle point along Mo–Pt phase diagram located MoPt (PDF 19–0809; *cP4*; AuCd–type,  $a_{\text{ref}} = 4.47 \text{ \AA}$ ;  $b_{\text{ref}} = 2.74 \text{ \AA}$ ;  $c_{\text{ref}} = 4.89 \text{ \AA}$ ) arises as a monophasic *fcc* system (Fig. 8). The Rietveld refinement reveals that all of the observed reflections are described with such a crystal structure. However, the observed intensities does not appear in accordance with the structure as being caused by the presence of preferred orientation, the filling of the atomic sites in the lattice, or as a combination of both of them.

Meanwhile, the present MoPt<sub>2</sub> sample arises as a rather complicated crystal structure since the peak widths of XRD–reflections reveal the presence of more

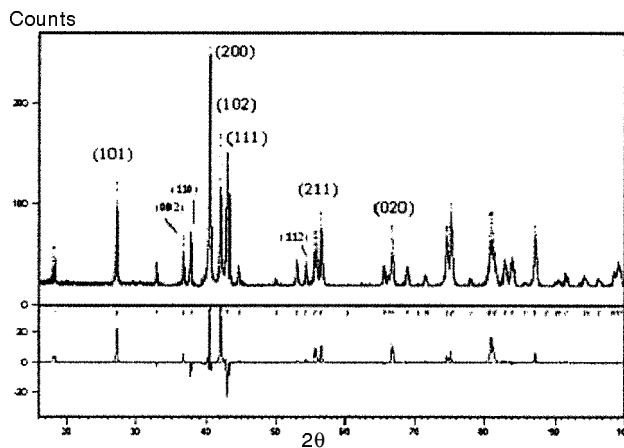


Figure 8. XRD diffractogram of MoPt specimen along with Rietveld correction.

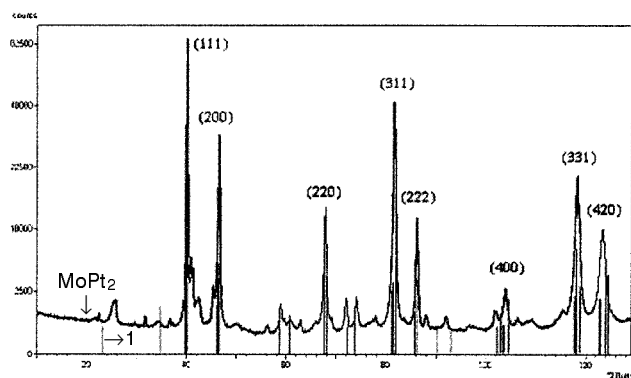


Figure 9. XRD diffractograms of MoPt<sub>2</sub> along with reference states of pure Pt and  $\beta$ -MoPt<sub>3</sub> specimens (all the lines below XRD curve; only one signed by 1).

than one phase (Fig. 9). Its MoPt<sub>2</sub> intermetallic phase has not been identified. As in the previous specimens, the most intense reflections are well described with an *fcc* phase, e.g. Pt. However, more reflections can be explained as a pseudocubic tetragonal cell with four atoms assumed in the unit cell,  $\beta$ -MoPt<sub>3</sub>, as a deformed Pt structure AuCu–type with superlattice reflections (PDF 17–0719; *tP4*;  $a = 4.90 \text{ \AA}$ ,  $c = 3.94 \text{ \AA}$ ). Since such a structure does not explain all of the visible reflections, perhaps traces of Mo (PDF 42–1120, *c/2*;  $a = 3.15 \text{ \AA}$ ) is present. In other words, since MoPt<sub>2</sub> does not exist as a stable Laves phase, natural tendency towards the most stable MoPt<sub>3</sub> phase and strong segregation effect of the *bcc* structure of Mo shift the whole complex system from its basic monophasic structure.

Samples with smaller Pt atomic percentage, in particular Mo<sub>4</sub>Pt, that are otherwise less important from a priority electrocatalytic point of view, characterizes larger lattice parameters and less small reflections (peaks shifted towards lower  $2\theta$  values) as far as the strong *fcc* reflections are considered (Fig. 10). The observed reflections are largely explained by the presence of *bcc* Mo (PDF 4–1120; *c/2*;  $a_{\text{ref}} = 3.15 \text{ \AA}$ ) and *hcp* Mo<sub>3</sub>Pt<sub>2</sub> (PDF 17–0710; *hP8*;  $a_{\text{ref}} = 2.82 \text{ \AA}$ ;  $c_{\text{ref}} = 4.53 \text{ \AA}$   $\delta$ -phase Ni<sub>3</sub>Sn–type), since the segregation

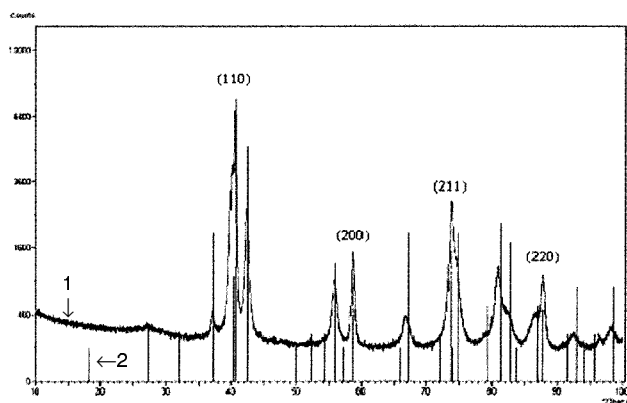


Figure 10. XRD diffractograms of  $\text{Mo}_4\text{Pt}$  specimen (1) along with pure Mo and  $\text{Mo}_3\text{Pt}_2$  (all the lines below XR curve; only one signed by 2). Indicated peaks relates Mo reflections.

increases with increasing atomic percentage of Mo [23–25]. In all specimens with prevailing Mo content reflections of  $\text{Mo}_3\text{Pt}_2$  structure are visible; this sample has an extra reflection with a  $d$ -value of 3 Å, alike  $\text{MoPt}_3$ . All of the identified phases are based almost entirely on the lattice peak positions, and not on the measured intensities.

The XRD conclusion is that only stable and symmetric Laves phases of high enthalpies of formation provide perfect homogenous monophase polycrystalline lattice, and even superlattice, and fortunately, these (stable  $\text{MoPt}_3$ , and metastable  $\text{MoPt}_4$ ) are only of significance in electrocatalysis for the HER. Between *bcc* of Mo and *fcc* of Pt, there is a broad interelectronic space of missing *hcp* structure [18,19], so that in all other alloying combinations, while maintaining any of defined overall chemical composition, there is a strong natural tendency towards segregation usually between stable Laves phases and individual elements [29,30]. From such a viewpoint the intermetallic phase of richer Mo and depleted in Pt content,  $\text{Mo}_3\text{Pt}_2$  itself, might be of particular electrocatalytic interest and significance.

### Kinetic Properties of Mo–Pt intermetallic Phases and Alloys

To assess most active specimens and distribution of electrocatalytic activity for the HER, kinetic examination has been carried out all along the Mo–Pt phase diagram. Such an integral presentation of steady-state polarization properties scanned with non-activated specimens is summed-up in Fig. 11. Presented results show the existence of two Tafel slopes for all samples, except MoPt. The kinetic parameters for all alloys are displayed in Table 1. All electrodes feature almost ideal Tafel slope of  $30 \text{ mV dec}^{-1}$  all along to the broader initial range until 100 and  $200 \text{ mA cm}^{-2}$  ( $E > -0.050 \text{ V vs. RHE}$ ), and obey Volmer–Tafel mechanism with the Tafel or catalytic recombination reaction as the RDS [12]. At higher cathodic reaction rates ( $E < -0.150 \text{ V vs. RHE}$ ), all electrodes follow Volmer–Heyrowski mechanism with Heyrowski reaction of electrochemical desorption as the RDS, while  $\text{MoPt}_3$  and  $\text{MoPt}_4$  feature

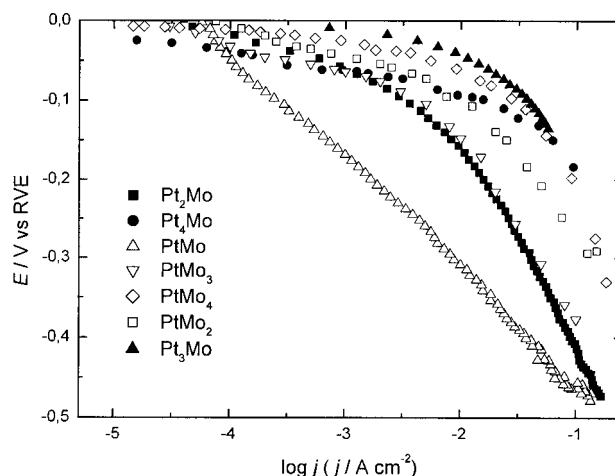


Figure 11. Tafel plot displays for the HER on intermetallic phases and alloys (as indicated), taken along Mo–Pt phase diagram.

Table 1. Kinetic parameters for HER on alloys and intermetallic phases along Mo–Pt phase diagram.

Electrode	$-b_1/\text{V dec}^{-1}$	$-b_2/\text{V dec}^{-1}$	$j_0/\text{A cm}^{-2}$	$j/\text{A cm}^{-2}$ ( $E = -0.2 \text{ V vs. RHE}$ )
$\text{Mo}_4\text{Pt}$	0.028	0.142	$1.0 \cdot 10^{-4}$	0.100
$\text{Mo}_3\text{Pt}$	0.037	0.230	$1.8 \cdot 10^{-5}$	0.0178
$\text{Mo}_2\text{Pt}$	0.036	0.180	$6.3 \cdot 10^{-5}$	0.0436
MoPt	–	0.140	$6.2 \cdot 10^{-5}$	0.0015
$\text{MoPt}_2$	0.038	0.250	$4.0 \cdot 10^{-5}$	0.0158
$\text{MoPt}_3$	0.028	0.117	$1.8 \cdot 10^{-4}$	0.292
$\text{MoPt}_4$	0.028	0.118	$1.0 \cdot 10^{-5}$	0.162

the most regular behavior ( $120 \text{ mV dec}^{-1}$ ). The latter implies H-adatoms surface coverage of constant value ( $H_{\text{ads}} = H_{\text{OPD}}$ ,  $\Theta_{\text{H}} \approx \text{const.}$ ), relative to the overall electrocatalytic rate of the HER. The main observation is that the higher the Pt content, the higher arises the electrocatalytic activity. Such a hierarchy disturbs only the specimen the most rich in atomic Mo content ( $\text{Mo}_4\text{Pt}$ ), for which XRD analysis reveals the prevailing content of the *hcp*  $\text{Mo}_3\text{Pt}_2$  intermetallic phase, which as a stable Laves intermetallic phase is expected contribute to the higher catalytic activity [2,3]. Such a state of experimental evidence suggests nanostructured electrocatalysts of lower (2–4 nm) particle size, to keep actual current density at least for two orders of magnitude lower versus the one calculated upon the projected surface geometric area and this way extend the reversible potential range to apparently higher current densities.

In such a respect, the survey of scanned electrocatalytic activity along Mo–Pt phase diagram for the reversible and irreversible potential range display two typical volcano plots in Fig. 12 and Fig. 13, respectively. Both volcanic plots appear asymmetric and do not fully coincide either with work function measurements (Fig. 5), or to the shift in bonding peak from XPS measurements (Fig. 3). However, these correspond to other formerly examined hypo–hyper–

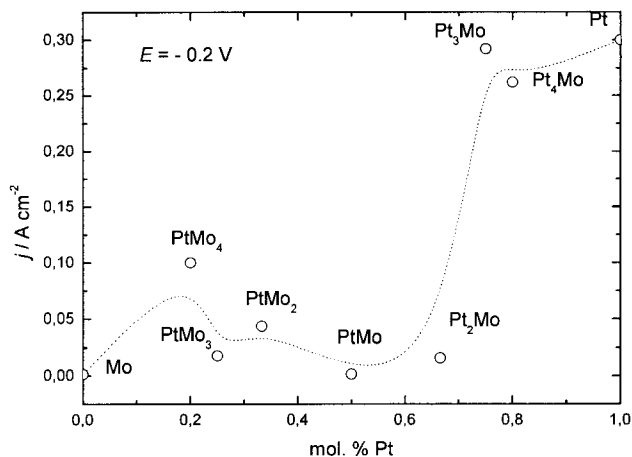


Figure 12. Relative electrocatalytic activity display for various electrodes taken along Mo–Pt phase diagram, and expressed as current density values at constant potential in the HER (higher polarization range).

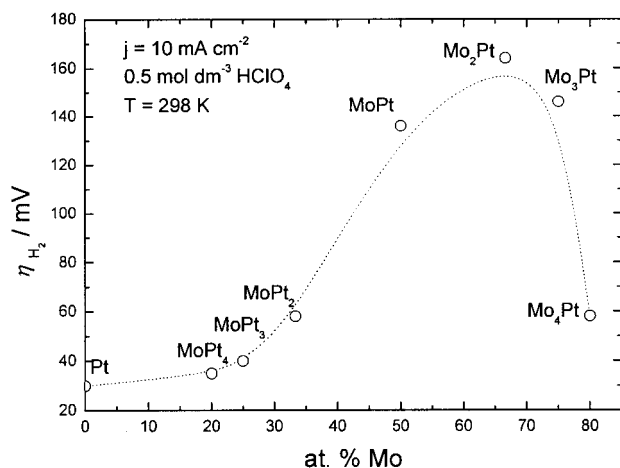


Figure 13. Relative electrocatalytic activity display for various electrodes taken along Mo–Pt phase diagram, and expressed as overpotential values at constant current density in the HER (low polarization range).

*d*-interelectronic combinations of transition metals (Zr–Ni, Mo–Ni, Ti–Ni, etc.) [3,26,27], and, as theoretically predicted [3,26,27,31], arises characteristic for the other ones. Such a collective comparable display reveals the entire sense of such a model system in electrocatalysis.

To complete the picture, Fig. 14 presents polarization properties of activated and non-activated MoPt<sub>3</sub> electrode for the HER, where the former implies fine polishing (down to 0.05 (m degree) to remove MoO<sub>3</sub> from the exposed surface for electrochemical process. The result is a remarkable extension of the reversible Volmer–Tafel range in 30 mV dec<sup>-1</sup> Tafel slope. Upon a RDE with fresh activated specimen such reversible interval extends even much further and enters within and above the current density values of A·cm<sup>-2</sup>, that means and defines the superactive state of electrocatalyst, or, in other words, an almost ideal electrocatalytic behavior. Measurements in ac impedance have revealed [12] that while the coverage of non-activated MoPt<sub>3</sub> and MoPt<sub>4</sub>

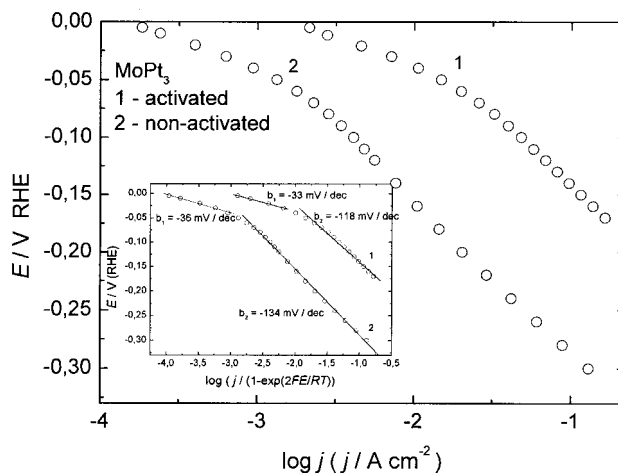


Figure 14. Polarization curves and corresponding Tafel plots for the HER at MoPt<sub>3</sub> electrode in 0.5 M HClO<sub>4</sub> at 298.15 K: (1) – activated and (2) non-activated electrodes, both being prepolarized at constant cathodic potential (– 0.150 V vs. RHE).

electrodes at steady state of HER feature only 30% H-atom coverage of available active centers ( $\Theta_{\text{H}} \approx 0.3$ ), the activated electrocatalysts approach 95% and even more of the value characteristic for pure polycrystalline Pt ( $\Theta_{\text{H}} \approx 0.95$ ). Such state of experimental evidence suggests either that Mo is located in the center of primary tetrahedral crystal unit of MoPt<sub>3</sub> and thereby the exposed surface consists only of ordered Pt atoms, or that interbonding hypo–hyper–*d*-interelectronic effect succeeds to provide some unique interorbital structure. In such intermetallic composite, even Mo, which as a individual metal does not adsorb H-atoms, features mutual properties of such a stoichiometric compound. As already mentioned, one possibility to persist within the reversible range of Tafel catalytic desorption step, would be to increase for two or more order of magnitudes the actual versus apparent surface area and keep electrode in the reversible potential ranger. The other ways of continuous cleaning of exposed surface from MoO<sub>3</sub> deposit are the subject of further studies.

#### ACKNOWLEDGEMENTS

This paper has been supported by and carried out within EU Project 'Prometheas', Contract Nr. ICA2-2001-10037, and EU Project 'Apollon', Contract Nr. ENK5-CT-2001-00572, EU Project Nr. NNE5-2001-00187. Authors feel their kind gratuities to Professor P. L. H. Notten, Philips Research Laboratory, Eindhoven, the Netherlands, for generous supply of properly metallurgically prepared and XRD tested standard monophase specimens along the Mo–Pt phase diagram.

#### REFERENCES

- [1] C. Song, *Catalysis Today*, **77** (2002) 17.
- [2] M.M. Jakšić, *Electrochim. Acta*, **29** (1984) 1539.
- [3] M.M. Jakšić, *J. Mol. Catalysis*, **38** (1986) 161.
- [4] M. Watanabe, S. Motoo, *J. Electroanal.Chem.*, **60** (1975) 267.
- [5] K.L. Ley, R. Liu, C. Pu, Q. Fan, N. Leyarowska, C. Segre, E.S. Smotkin, *J. Electrochem. Soc.*, **144** (1997) 1543.
- [6] B. N. Grgur, G. Zhuang, N.M. Marković, P.N. Ross, *J. Phys. Chem. B*, **101** (1997) 3910.
- [7] B.N. Grgur, N.M. Marković, P.N. Ross, *J. Phys. Chem. B*, **102** (1998) 2494.
- [8] B.N. Grgur, N.M. Marković, P.N. Ross, *J. Electrochem. Soc.*, **146** (1999) 1613.

- [9] M.S. Ishikawa, M.S. Liao, C.R. Cabrera, *Surf. Sci.*, **513** (2002) 98.
- [10] V. Papaefthimiou, A. Siokou, S. Kennou, *J. Appl. Phys.*, **91** (2002) 4213.
- [11] H. Angerstein-Kozłowska, B. E. Conway, W. B. A. Sharp, *J. Electroanal. Chem.*, **43** (1973) 9.
- [12] A.J. Bard, L.R. Faulkner *Electrochemical Methods; Fundamentals and Applications*, chapter 9, Wiley, New York, p. 316, 1980.
- [13] J. Jakšić, Lj. Vračar, S.G. Neophytides, N. Krstajić, *J. New Mat. Electrochem. Systems*, **7** (2004) 205
- [14] Lj. Vračar, N. Krstajić, S.G. Neophytides, J. Jakšić, *Int. J. Hydrogen Energy*, **29** (2004) 835
- [15] J. Jakšić, N. Krstajić, Lj. Vračar, *Mater. Sci. Forum*, **453/454** (2004) 115.
- [16] S.G. Neophytides, S.H. Zafeiratos, M.M. Jakšić, *J. Electrochem. Soc.*, **150** (2003) E512.
- [17] S.G. Neophytides, S.H. Zafeiratos, M.M. Jakšić, *Chem. Ind.*, **57** (2003) 368.
- [18] L. Brewer, *Science*, **161** (1968) 115.
- [19] L. Brewer, in *Electronic Structure and Alloy Chemistry of Transition Elements*, P.A. Beck, Ed., Interscience, New York, p. 221, 1963.
- [20] F.R. De Boer, R. Boom, W.C.M. Mattens, A.R. Miedema, A.K. Niessen, *Cohesion and Structure*, F.R. De Boer, D.G. Pettifor, Eds., North Holland, Amsterdam, Vol. **1**, 1988.
- [21] J. Friedel, C.M. Sayers, *J. Phys.*, **38** (1977) 687.
- [22] J. Friedel, in *Physics in Metal I: Electrons*, Cambridge Univ. Press, Cambridge, p. 340, 1969.
- [23] Mavrikakis, M., Stoltze, P., Norskov, J.K., *Catal. Lett.*, **64** (2000) 101.
- [24] Christoffersen, E., Liu, P., Ruban, A., Skriver, H.L., Norskov, J.K.J. *Catalysis*, **199** (2001) 123.
- [25] Hammar, B.; Norskov, J. K. *Adv. Catalysis*, **45** (2000) 71.
- [26] M.M. Jakšić, *J. New Mat. Electrochem. Systems*, **3** (2000) 153.
- [27] M.M. Jakšić, *Electrochim. Acta*, **45** (2000) 4085.
- [28] L. Brewer, R.H. Lamoreaux, *Bulletin of Alloy Phase Diagrams*, **1** (1980) 89.
- [29] J.K. Gibson, L. Brewer, K.A. Gingerich, *Metal. Trans. A*, **15** (1984) 2075.
- [30] M.M. Jakšić, *High Temp. Sci.*, **30** (1990) 19.
- [31] S.G. Neophytides, S. Zafeiratos, G.D. Papakonstantinou, J.M. Jakšić, F.E. Paloukis, M.M. Jakšić, *Int. J. Hydrogen Energy*, **30** (2005) 131, 393.



### JELENA M. JAKŠIĆ

Jelena M. Jakšić graduated from the Faculty of Physical Chemistry, Faculties of Sciences, University of Belgrade in 1995, with two academic years of studies at the Departments of Physics and Chemical Engineering, University of Patras in Greece. Diploma thesis done with Professor Slavko Mentus on Non-Faradaic Electrochemical Modification of Catalytic Activity (NEMCA) for Heterogeneous Reaction of Hydrogen Oxidation in Aqueous Media was awarded "the Belgrade October city prize" for creative contribution of youth on 20<sup>th</sup> October 1997. M.S. studies at the Center for Multidisciplinary Studies, University of Belgrade, Surface State division, were completed in 2000 with Professors N. Krstajić, M. Vojnović and N. Ristić on Kinetics of Hydrogen Evolution on Intermetallic Phases and Alloys of Ni, Co and Mo. Ph.D. degree was earned in 2004 from the Faculty of Technology and Metallurgy, University of Belgrade with partial fulfillment at the University of Patras, Greece in the frame of two EU research projects, "Prometheas" and "Apollon", on Kinetics of electrochemical Hydrogen Evolution and Oxidation Reactions on Mo-Pt Alloys carried out with Professor Nedeljko Krstajić. She received a one-year Greek Ministry of science grant for work on doctoral thesis. So far together with her supervisors she has published 12 scientific papers in recognized international journals. Scientific interests include electrocatalysis for hydrogen and oxygen electrode reactions.



### LJILJANA VRAČAR

Full professor at the Department of Physical Chemistry and Electrochemistry at the Faculty of Technology and Metallurgy, University of Belgrade. Born (1949) in Cetinje. B.Sc.1972, M.Sc. 1975 and Ph.D 1984, at the Faculty of Technology and Metallurgy, University of Belgrade. Post-doctoral Research Fellow during 1985–1986 and Research Associate during 1989 at the Department of Chemistry University of Ottawa, Ottawa, Canada. Subjects of interest: metal deposition and dissolution, electrochemical kinetics and mechanism of electrode reactions at metals, alloys and glassy metals (electrochemical evolution of hydrogen and oxygen, electrochemical oxygen reduction, hydride formation), kinetics and thermodynamics of adsorption, development of primary and secondary electrochemical power sources.



### STYLIANOS NEOPHYTIDES

Dr S. Neophytides is principal researcher in the Institute of Chemical Engineering & High Temperature Chemical Processes (FORTH/ICE-HT) in Patras. He obtained his Ph.D. from the Department of Chemical Engineering of the University of Patras in 1990. The period 1988–1991 he worked in the Laboratory of Petrochemical Technology of the University of Gent in Belgium. He is co-author of more than 45 publications in international journals and 3 invited chapters in books. Since 1990 he has participated in more than 15 research programmes and as co-ordinator in more than 5. His current research activities are heterogeneous catalysis, electrochemistry, polymer electrolyte membrane and solid oxide fuel cells, chemical reaction engineering, applications of IR and X-ray spectroscopies in catalysis and electrocatalysis.



### NEDELJKO KRSTAJIĆ

Associate professor at the Department of Physical chemistry and Electrochemistry at the Faculty of Technology and Metallurgy, University of Belgrade. Born (1954) in Belgrade. B.Sc. degree 1978, M.Sc. 1981, and Ph.D. 1989 at the Faculty of Technology and Metallurgy, University of Belgrade. Post-doctoral Research Fellow during 1992–1993 at the Department of Physical Chemistry and Electrochemistry, University of Milan, Milan, Italy. Subject of interest: Kinetics and mechanism of electrode reactions (deposition/dissolution of metals, hydrogen, oxygen and chlorine evolution reactions, hydrogen oxidation reaction and oxygen reduction reaction), new electrode materials (activated titanium anodes, electroconducting polymers, metal-hydride electrodes), corrosion, corrosion protection, electro-organic synthesis, electrochemical power sources.